HHS Public Access

Author manuscript

Calcif Tissue Int. Author manuscript; available in PMC 2019 March 01.

Published in final edited form as:

Calcif Tissue Int. 2018 March ; 102(3): 348–357. doi:10.1007/s00223-017-0355-3.

A Murine Model for Human ECO Syndrome Reveals a Critical Role of Intestinal Cell Kinase in Skeletal Development

Mengmeng Ding[1,5], **Li Jin**[1], **Lin Xie**[1,3], **So Hyun Park**[2], **Yixin Tong**[2,4], **Di Wu**[2], **A. Bobby Chhabra**[1], **Zheng Fu**[2], and **Xudong Li**[1]

[1]Department of Orthopaedic Surgery, University of Virginia, 135 Hospital Dr., Charlottesville, VA 22908, USA

[2]Department of Pharmacology, University of Virginia, PO Box 800735, 1340 Jefferson Park Avenue, Charlottesville, VA 22908, USA

[3]Department of Orthopaedic Surgery, Wuhan Orthopaedic Hospital, Huazhong University of Science & Technology, Hubei 430030, China

[4]The Gastrointestinal Surgery Center, Tongji Hospital, Huazhong University of Science & Technology, Hubei 430030, China

[5]Department of Anesthesiology, Shengjing Hospital of China Medical University, Shenyang, China

Abstract

An autosomal-recessive inactivating mutation R272Q in the human intestinal cell kinase (*ICK*) gene caused profound multiplex developmental defects in human endocrine-cerebro-osteodysplasia (ECO) syndrome. ECO patients exhibited a wide variety of skeletal abnormalities, yet the underlying mechanisms by which ICK regulates skeletal development remained largely unknown. The goal of this study was to understand the structural and mechanistic basis underlying skeletal anomalies caused by ICK dysfunction. *Ick* R272Q knock-in transgenic mouse model not only recapitulated major ECO skeletal defects such as short limbs and polydactyly but also revealed a deformed spine with defective intervertebral disk. Loss of ICK function markedly reduced mineralization in the spinal column, ribs, and long bones. *Ick* mutants showed a significant decrease in the proliferation zone of long bones and the number of type X collagen-expressing hypertrophic chondrocytes in the spinal column and the growth plate of long bones. These results implicate that ICK plays an important role in bone and cartilage development by promoting chondrocyte proliferation and maturation. Our findings provided new mechanistic insights into the skeletal phenotype of human ECO and ECO-like syndromes.

Correspondence to: Zheng Fu; Xudong Li.

Compliance with Ethical Standards

Conflict of interest Mengmeng Ding, Li Jin, Lin Xie, So Hyun Park, Yixin Tong, Di Wu, A. Bobby Chhabra, Zheng Fu, Xudong Li declare that they have no conflict of interest.

Human and Animal Rights and Informed Consent All procedures involving animals were performed in accordance with ethical standards in an animal protocol that was approved by the Institutional Animal Care and Use Committee.

Electronic supplementary material The online version of this article (https://doi.org/10.1007/s00223-017-0355-3) contains supplementary material, which is available to authorized users.

Keywords

Intestinal cell kinase; Endocrine-cerebro-osteodysplasia syndrome; Bone development; Intervertebral disk; Hypertrophic chondrocyte

Introduction

Endochondral ossification is a stringently controlled and coordinated process during bone development, starting from mesenchymal stem cell condensation to form a template of future bone. Chondrocytes at both the proximal and distal ends of the template proliferate, while chondrocytes in the middle of the template differentiate into hypertrophic chondrocytes that secrete extracellular matrix (ECM). Hypertrophic chondrocytes eventually undergo apoptosis, and leave the cartilaginous matrix scaffold that attracts osteoblasts to form the primary spongiosa [1, 2].

Primary cilium, a microtubule-based organelle, has been implicated an important role in the skeletal development and homeostasis [3]. Mutations interfering with formation and maintenance of primary cilia were identified in skeletal ciliopathies, including Ellis–van Creveld syndrome (EVC), cranioectodermal dysplasia (CED), asphyxiating thoracic dystrophy (ATD), short rib-polydactyly syndrome (SRPS), and endocrine-cerebro-osteodysplasia (ECO) syndrome [4]. Intestinal cell kinase (ICK) is a highly conserved and ubiquitously expressed serine/threonine protein kinase that plays an important role in the maintenance of primary cilia. Several missense point mutations in the human *ICK* gene, including c.1305G-A (R272Q), c.358G-T (G120C), and c.238G-A (E80 K), were reported in ECO and ECO-like syndromes. R272Q and G120C have been confirmed to be loss of function mutations because they impaired ICK catalytic activity and subcellular localization [5, 7]. These neonatal lethal autosomal-recessive human disorders displayed profound skeletal abnormalities such as poly-dactyly, short ribs, bowed limbs, and abnormal long bones [5–9].

Our prior work has demonstrated an important role for ICK in the regulation of cell proliferation and survival in vitro [10, 11]. An essential role of ICK in vivo emerged from the report of human ECO and ECO-like syndromes [5–7]. Recently, *Ick* knockout mouse models reproduced ECO phenotypes in the cerebral and skeletal systems and linked ICK deficiency to abnormal structures of primary cilia [7–9]. However, cellular and molecular mechanisms of ICK in ECO phenotypes are still elusive. To understand the mechanistic basis of ECO developmental anomalies, we generated an *Ick* R272Q knock-in mouse model that can recapitulate ECO developmental phenotypes in the lung [12]. Here, we analyzed the fetal bones of *Ick* R272Q mutant embryos with respect to ECO skeletal phenotype. Our results suggest that ICK plays a critical role in the development of skeleton and intervertebral disk (IVD) by regulating chondrocyte maturation and bone mineralization.

Materials and Methods

Ick^{R272Q} Mutant Mouse Model for Human ECO Syndrome

All procedures involving animals were performed in accordance with ethical standards in an animal protocol that was approved by the Institutional Animal Care and Use Committee. The R272Q (CGA > CAA) point mutation was introduced into the exon 8 of the wild type (WT) *Ick* allele on a bacterial artificial chromosome (BAC) to generate *Ick*/R272Q BAC [12]. A LNL (LoxP-Neo-LoxP) cassette was inserted in the intron downstream of exon 8. A gene targeting vector was constructed by retrieving the 5 kb long homology arm (5′ to LNL), the LNL cassette, and the 2 kb short homology arm (3′ to LNL) into a plasmid vector carrying the DTA (diphtheria toxin alpha chain) negative selection marker. The LNL cassette conferred G418 resistance during gene targeting in PTL1 (129B6 hybrid) ES cells and the DTA cassette provided an autonomous negative selection to reduce the random integration event during gene targeting. Several targeted ES cell clones were identified and injected into C57BL/6 blastocysts to generate chimeric mice. Male chimeras were bred to homozygous EIIa (cre/cre) females (in C57BL/6J background) to excise the neo cassette and to transmit the *Ick*/R272Q allele through germline (Precision Targeting Lab, USA). *Ick*^{R272Q} heterozygous were normal and intercrossed to produce *Ick*^{R272Q} homozygous embryos. Animals were housed in a temperature controlled colony room on a 12- hour light cycle, and had access to food and water ad libitum. For timed pregnancy, the presence of a copulation plug in the morning represented embryonic day (E) 0.5. Pregnant mice were euthanized by CO_2 inhalation and embryos were harvested at different developmental time points (n = 2–5).

Whole Mount Skeletal Staining

Embryos at E15.5 or E18.5 were placed in PBS after euthanization. The skin, internal organs, and bubbles were removed from the body cavity, and then fixed in 95% ethanol. Cartilages were stained with Alcian blue and bones were stained with Alizarin S red following a standard protocol [13]. After clearing, samples were placed in 100% glycerol for long-term storage and imaging (Olym-pus SZX12, Olympus).

Alcian Blue and Picrosirius Red Staining

Embryos were washed with PBS and fixed in 100% ethanol overnight. Paraffin embedded sections (5 μm) were subjected to 1% Alcian blue (pH 2.5) and Picrosirius red (0.1% Sirius red in saturated aqueous picric acid) staining. Images were taken with a Nikon Eclipse E600 microscope. Five semi-serial sections (10 μm between each level) through the center of femurs and spine from each embryo were cut, stained, and photographed for measurement using an NIS element BR imaging software (Nikon, Japan). Quantification data of histologic images were obtained as indicated in Online Resource 1.

von Kossa Staining

Paraffin embedded sections were dewaxed and incubated in 5% silver nitrate solution (w/v, Sigma, MO) under UV light for 30 min. Sections were rinsed in distilled water and immersed in 5% sodium thiosulfate (Sigma, MO) for 5 min and counterstained with

hematoxylin (Sigma) for 5 min. Quantification data of histologic images were obtained as indicated in Online Resource 1.

Immunohistochemistry

Immunostaining for paraffin sections was performed as described previously [14, 15]. For collagen X (GTX105788, 1:400, GeneTex, CA) and collagen II (CB11, 1:100, Chondrex, WA) staining, sections were treated with 2% bovine testicular hyaluronidase 30 min for antigen retrieval. The standard 3,3′-diaminobenzidine (DAB) procedure was followed to visualize the signal. Hematoxylin was used for counter-staining. IgG control was performed following identical procedures excluding the primary antibody.

Micro-computed Tomography (micro-CT)

Embryos at day 18.5 were fixed in 10% formalin. Micro-CT scans were performed on a micro-CT 80 scanner (70 kV, 114 μA; Scanco Medical, Switzerland), and then were reconstructed with an isotropic voxel size of 10 μm [16]. Multi-level threshold procedure (threshold for bone = 225) was applied to discriminate soft tissue from bone. Three-dimensional images were acquired for qualitative evaluation in an X-ray image mode.

Statistical Analysis

Histological quantification data were expressed as mean ± SEM. Statistical comparison between genotypes was performed by a two-tailed student's *t* test. $p < 0.05$ was considered significant.

Results

Overall Morphological Defects in *Ick*^{R272Q} Homozygous Mutant Embryos

Consistent with *Ick* R272Q being an autosomal-recessive inactivating mutation in ECO syndrome, *Ick*$^{R272Q/+}$ heterozygous mice were phenotypically indistinguishable from WT littermates. *Ick*$^{R272Q/+}$ heterozygotes were interbred to generate *Ick*$^{R272Q/R272Q}$ homozygotes that succumbed to death shortly after birth due to respiratory failure [12]. Embryos from *Ick*$^{R272Q/+}$ interbreed were harvested at E15.5 and E18.5. Gross morphology of *Ick*$^{R272Q/R272Q}$ mutants was remarkably distinct from that of WT or heterozygous mutant littermates. Compared with WT, *Ick* R272Q homozygous mutants had a broader head, smaller nose, bigger mouth, and shorter thorax (Fig. 1a). They also displayed broader cervical flexure, shorter distance between lower jaw to the forelimb, and larger abdominal cavity, flat ankles, and flat neck-spine angles (Fig. 1). These features closely resemble the clinical manifestations of ECO syndrome [9]. In addition to reported ECO skeletal phenotypes, these mutant mice also exhibited severe structural defects in the spinal column (Figs. 1b, 2b).

Expression of ICK in the Skeletal System

Previously, we showed that ICK is ubiquitously expressed in mouse tissues [17]. We examined ICK expression in bone and cartilage tissues by Western blotting and by β-galactosidase staining of an *Ick-LacZ* reporter mouse. As shown in Online Resource 2A,

ICK protein was detected in tibia, sternum, and rib as well as in lung and heart. A truncated *Ick* transcript fused with *LacZ* was expressed in $Ick^{tm1a/+}$ heterozygotes (from NIH Knockout Mouse Project Repository) [9], thus LacZ staining can be used to map ICK expression in mouse tissues. In Online Resource 2B, LacZ staining of E15.5 whole embryos revealed ICK expression in limbs and spine.

Skeletal Defects in Ick^{R272Q} Homozygous Mutant

To further investigate the role of ICK in bone and cartilage, whole mount skeletal analysis was performed on *Ick* mutant embryos. The skeletal phenotypes of $Ick^{R272Q/R272Q}$ include short limbs, polydactyly, bowed long bones, and much less bone mineralization than WT (Fig. 2a). At E15.5, limb and tarsal bones of *Ick* mutants were all deformed; the longitudinal length of long bones was significantly reduced, and polydactyly was evident in both forelimb and hindlimb (average 6.5 digits) as compared with WT littermates (Fig. 2a). The proportion of mineralized bone (red) in the long bones was significantly reduced as compared with WT (Online Resource 3). A striking new discovery made in our *Ick* mutant mouse model that was not previously detailed in pathological reports of ECO patients and *Ick* null mice is the dramatic deformation of the spine (Fig. 2b). Compared with WT, the vertebrae and transverse processes of *Ick* mutants were severely distorted as shown by whole mount skeletal staining and micro-CT at E18.5 (Fig. 2b). Underdeveloped rib cage may not support the initial breath after birth.

Abnormal Phenotype of Growth Plate and Intervertebral Disk

Histological analyses were performed on femurs (Fig. 3) and spines (Fig. 4) of E15.5 and E18.5 embryos. *Ick* mutant femur was significantly shorter than WT femur at E18.5 (Fig. 3d). While the size of cartilage region of *Ick* mutant femur was not significantly different from that of WT femur, endochondral bone of *Ick* mutants was barely detectable in E15.5 femurs and at least 50% shorter than that of WT in E18.5 femurs (Fig. 3). The relative length of the proliferating chondrocyte (PC) zone normalized to PC and the resting chondrocyte (RC) zone was significantly shorter in *Ick* mutants than in WT littermates (Fig. 3c). von Kossa staining confirmed much less matrix mineralization in *Ick* mutant femurs than in WT femurs at E15.5 and E18.5 (Fig. 5a–d, i).

In *Ick* mutant embryos, the vertebrae appeared deformed and the IVD was defective (Fig. 4). Compared with WT, vertebrae of *Ick* mutants were much narrower, irregularly shaped, and severely distorted. A significant reduction of mineralization in the spinal column of *Ick* mutants at E18.5 was shown by quantification of von Kossa staining (Fig. 5e–h, i).

Impaired Chondrocyte Maturation in *Ick* Mutant Skeletal System

Hypertrophic chondrocytes play an important role in bone mineralization. To determine whether reduced mineralization of *Ick* mutant skeleton was due to compromised chondrocyte maturation, we performed immunostaining in E15.5 femur and spine to compare the expression of type X collagen, a specific marker for terminally differentiated hypertrophic chondrocytes as well as type II collagen, a marker for chondrocytes. Type X collagen was expressed in the hypertrophic regions and ECM of long bones (Fig. 6c, brown), and vertebrae (Fig. 6g) in WT embryos. Compared with WT, long bones (Fig. 6d) and

vertebrae (Fig. 6h) of *Ick* mutants expressed type X collagen in the hypertrophic regions at a significantly reduced level. In E15.5 WT femurs, type II collagen was primarily expressed in the resting and proliferative chondrocytes and ECM (Fig. 6a, Online Resource 5). In E15.5 *Ick* mutant femurs, type II collagen was expressed throughout the resting and proliferative zones and into the hypertrophic region (Fig. 6b). In WT spine, collagen type II expressed abundantly in annulus fibrosus (AF) tissue and proliferating chondrocytes (Fig. 6e). In *Ick* mutant spine, IVDs were underdeveloped, without clear structure of nucleus pulposus (NP) and AF, and collagen II expression was observed in proliferating and hypertrophic zones (Fig. 6f). These results together indicate that ICK dysfunction significantly impairs chondrocyte maturation in both spine and long bones.

Discussion

ECO is a rare recessive genetic disorder caused by a homozygous loss of function mutation R272Q or G120C in the human *ICK* gene [5, 6]. ECO syndrome displays significant skeletal phenotypes such as polydactyly and micromelia [5]. Recent studies from *Ick* knockout mice confirmed ECO skeletal phenotypes including polydactyly, short limbs, distorted, and shortened long bones [9]. Alcian blue/Alizarin red staining of *Ick* knockout E18.5 embryos indicated reduced bone ossification [9]. Using an innovative ECO mutation knock-in mouse model, we herein reported the following significant findings. First, our ECO mutation R272Q knock-in model confirmed major skeletal defects reported in ECO patients [5, 6] and *Ick* knockout mice [9]. Additionally, we discovered significant structural anomalies in the spine of both *Ick* R272Q mutants (Figs. 2, 4) and *Ick* null mutants (Online Resource 4), manifested as distorted spine column and defective intervertebral disk. This observation is consistent with the radiograph results showing mildly defective ossification of the vertebrae in ECO patients that carry homozygous *ICK* G120C mutation [6]. Furthermore, using von Kossa staining, we demonstrated reduced mineralization in long bones as a result of ICK dysfunction. Similar to our loss of function mutant strain, *Ick* knockout mice described by Moon et al. [9] showed delayed ossification in the digits, short limbs, and reduced bone mineralization at E18.5.

$Ick^{R272Q/R272Q}$ mutant revealed a marked disruption of growth plate architecture with a reduction in proliferative chondrocyte zone, consistent with what was observed earlier in *Ick* null mutant [7]. Although the hypertrophic chondrocyte zone of $Ick^{R272Q/R272Q}$ is not significantly different from that of WT, the number of hypertrophic chondrocytes expressing collagen X, a specific marker for terminally differentiated hypertrophic chondrocytes, is dramatically reduced in *Ick* mutants as compared with their WT littermates. This observation is in agreement with a severe deficiency in calcified cartilage matrix and a significant delay of mineralization in the long bone and spinal ossification center of *Ick* mutants. In the final step of chondrocyte differentiation, the cartilaginous matrix is replaced by mineralized matrix [18]. Hypertrophic chondrocyte terminal differentiation is a critical step in mineralization. This developmental process requires stringent control mechanisms including action of hormones, morphogens, ECM proteins as well as transcriptional factors [19, 20]. There are common factors that regulate both chondrocyte maturation and bone calcification [21]. Compared with WT littermates, *Ick* mutant embryos showed a higher expression of collagen II in hypertrophic zone concomitant with a much lower type X

collagen expression in the ossification center. These results provide new evidence for an essential role of ICK in chondrogenic cell differentiation and maturation during skeletal development.

Our in vitro cell-based studies have suggested that ICK signaling is pro-proliferation and pro-survival [10, 11]. It is, therefore, conceivable that the significant decrease in the size of proliferation zone and the number of type X collagen-expressing hypertrophic chondrocytes could be due to elevated rates of cell death of certain cell types rather than impaired proliferation and/or differentiation of chondrocytes in the growth plate. To test this hypothesis, we conducted immunostaining of apoptotic cells using cleaved PARP and caspase-3 antibodies. We observed a low number of apoptotic cells and no significant difference in the percentage of labeled apoptotic cells between normal and *Ick* mutant growth plates (data not shown). Given the experimental difficulty in assessing cell death based on a low number of cells undergoing this process, we cannot completely exclude the possible contribution of aberrant cell apoptosis to the abnormal architecture of cartilage growth plates in *Ick* mutants. However, data from both *Ick* R272Q mutant and *Ick* null models [7] seem to suggest that defects in cellular events involving proliferation and chondrocyte differentiation may be the primary causes for alterations in proliferative and hypertrophic zones of cartilage growth plates in ECO syndrome.

A striking new skeletal phenotype of ECO syndrome identified in *Ick* R272Q mutant is the defect of IVD. IVD consists of gelatinous NP in the center, surrounded by fibrocartilaginous AF, and superior and inferior cartilaginous endplates. NP is believed to be derived from the notochord while AF and endplate are developed from sclerotome [22]. Notochord formation is the foundation of the disk development because notochord is a crucial signaling center for the paraxial mesoderm that gives rise to the sclerotome and subsequently fibrous AF tissue and cartilage endplate of IVD [23, 24]. NP is apparent by E15.5 as shown in Fig. 4a, a′, composed of notochordal cells and large vacuolated cells. Disruption of notochord formation and/or sclerotome specification can lead to a much smaller or completely absence of IVD. Thus, the underdevelopment of IVD in *Ick* mutant spine strongly implicates an essential role for ICK in the determination of early notochord and sclerotome formation.

ICK has a well-established role in regulating the length of primary cilia. The primary cilium is a signaling nexus for growth plate function and skeletal development [25]. In *Ick* null mice, impaired Hedgehog signaling has been linked to abnormal limb patterning and skeletal development caused by ICK dysfunction [7, 9]. Despite the strong correlative evidence from the *Ick* knockout mouse model, a functional relationship between Hedgehog signaling and the ECO skeletal phenotypes has yet to be established. Since the primary cilium can regulate many other signaling pathways (Wnt, TGFβ, FGF, and Notch), a more significant question to address in our future studies is how ICK coordinate various signaling events in the primary cilium to control chondrocyte maturation and endochondral ossification.

There are some similarities between WT E15.5 images and R272Q E18.5 images (Fig. 3a vs 3c). We recognize that one limitation of our current study is that we could not address whether the skeletal phenotype we observed in our ECO R272Q mutant mouse model is due to delayed developmental process or developmental failures. Since our current global R272Q

homozygous knock-in mice die at birth due to respiratory distress [12], inducible tissue-specific R272Q knock-in or *Ick* null mouse model is required to allow postnatal analyses of bone phenotype in ECO mutants.

In summary, we have shown that *Ick* R272Q knock-in mouse model resembles the skeletal abnormalities of human ECO syndrome, and ICK plays an important role in bone and IVD development, possibly by regulating chondrocyte proliferation, differentiation, and maturation.

Supplementary Material

Refer to Web version on PubMed Central for supplementary material.

Acknowledgments

We are grateful for the partial financial support from NIH R01AR064792 (XL), DK082614 (ZF), and CA195273 (ZF). We appreciate the technical assistance of the Research Histology Core at University of Virginia. The funders have no role in the study.

References

1. Kronenberg HM. Developmental regulation of the growth plate. Nature. 2003; 423:332–336. [PubMed: 12748651]
2. Olsen BR, Reginato AM, Wang W. Bone development. Annu Rev Cell Dev Biol. 2000; 16:191–220. [PubMed: 11031235]
3. Serra R. Role of intraflagellar transport and primary cilia in skeletal development. Anat Rec (Hoboken). 2008; 291:1049–1061. [PubMed: 18727103]
4. Badano JL, Mitsuma N, Beales PL, Katsanis N. The ciliopathies: an emerging class of human genetic disorders. Annu Rev Genomics Hum Genet. 2006; 7:125–148. [PubMed: 16722803]
5. Lahiry P, Wang J, Robinson JF, Turowec JP, Litchfield DW, Lanktree MB, Gloor GB, Puffenberger EG, Strauss KA, Martens MB, Ramsay DA, Rupar CA, Siu V, Hegele RA. A multiplex human syndrome implicates a key role for intestinal cell kinase in development of central nervous, skeletal, and endocrine systems. Am J Hum Genet. 2009; 84:134–147. [PubMed: 19185282]
6. Oud MM, Bonnard C, Mans DA, Altunoglu U, Tohari S, Ng AY, Eskin A, Lee H, Rupar CA, de Wagenaar NP, Wu KM, Lahiry P, Pazour GJ, Nelson SF, Hegele RA, Roepman R, Kayserili H, Venkatesh B, Siu VM, Reversade B, Arts HH. A novel ICK mutation causes ciliary disruption and lethal endocrine-cerebro-osteodysplasia syndrome. Cilia. 2016; 5:8. [PubMed: 27069622]
7. Paige TS, Kunova BM, Varecha M, Balek L, Barta T, Trantirek L, Jelinkova I, Duran I, Vesela I, Forlenza KN, Martin JH, Hampl A, Bamshad M, Nickerson D, Jaworski ML, Song J, Ko HW, Cohn DH, Krakow D, Krejci P. An inactivating mutation in intestinal cell kinase, ICK, impairs hedgehog signalling and causes short rib-polydactyly syndrome. Hum Mol Genet. 2016; 25:3998–4011. [PubMed: 27466187]
8. Chaya T, Omori Y, Kuwahara R, Furukawa T. ICK is essential for cell type-specific ciliogenesis and the regulation of ciliary transport. EMBO J. 2014; 33:1227–1242. [PubMed: 24797473]
9. Moon H, Song J, Shin JO, Lee H, Kim HK, Eggenschwiller JT, Bok J, Ko HW. Intestinal cell kinase, a protein associated with endocrine-cerebro-osteodysplasia syndrome, is a key regulator of cilia length and Hedgehog signaling. Proc Natl Acad Sci USA. 2014; 111:8541–8546. [PubMed: 24853502]
10. Fu Z, Kim J, Vidrich A, Sturgill TW, Cohn SM. Intestinal cell kinase, a MAP kinase-related kinase, regulates proliferation and G1 cell cycle progression of intestinal epithelial cells. Am J Physiol Gastrointest Liver Physiol. 2009; 297:G632–G640. [PubMed: 19696144]

11. Bolick DT, Chen T, Alves LOA, Tong Y, Wu D, Joyner LT 2nd, Oria RB, Guerrant RL, Fu Z. Intestinal cell kinase is a novel participant in intestinal cell signaling responses to protein malnutrition. PLoS ONE. 2014; 9:e106902. [PubMed: 25184386]
12. Tong Y, Park SH, Wu D, Xu W, Guillot SJ, Jin L, Li X, Wang Y, Lin CS, Fu Z. An essential role of intestinal cell kinase in lung development is linked to the perinatal lethality of human ECO syndrome. FEBS Lett. 2017; 591:1247–1257. [PubMed: 28380258]
13. Rigueur D, Lyons KM. Whole-mount skeletal staining. Methods. Mol Biol. 2014; 1130:113–121.
14. Xiao L, Ding M, Zhang Y, Chordia M, Pan D, Shimer A, Shen FH, Glover D, Jin L, Li X. A novel modality for functional imaging in acute intervertebral disc herniation via tracking leukocyte infiltration. Mol Imaging Biol. 2017
15. Jin L, Liu Q, Scott P, Zhang D, Shen FH, Balian G, Li X. Annulus fibrosus cell characteristics are a potential source of intervertebral disc pathogenesis. PLoS ONE. 2014; 9:e96519. [PubMed: 24796761]
16. Xiao L, Ding M, Fernandez A, Zhao P, Jin L, Li X. Curcumin alleviates lumbar radiculopathy by reducing neuroinflammation, oxidative stress and nociceptive factors. Eur Cell Mater. 2017; 33:279–293. [PubMed: 28485773]
17. Chen T, Wu D, Moskaluk CA, Fu Z. Distinct expression patterns of ICK/MAK/MOK protein kinases in the intestine implicate functional diversity. PLoS ONE. 2013; 8:e79359. [PubMed: 24244486]
18. Karsenty G, Wagner EF. Reaching a genetic and molecular understanding of skeletal development. Dev Cell. 2002; 2:389–406. [PubMed: 11970890]
19. Horton WA. Skeletal development: insights from targeting the mouse genome. Lancet. 2003; 362:560–569. [PubMed: 12932391]
20. Breur GJ, Farnum CE, Padgett GA, Wilsman NJ. Cellular basis of decreased rate of longitudinal growth of bone in pseudoachondroplastic dogs. J Bone Joint Surg Am. 1992; 74:516–528. [PubMed: 1583046]
21. Michigami T. Regulatory mechanisms for the development of growth plate cartilage. Cell Mol Life Sci. 2013; 70:4213–4221. [PubMed: 23640571]
22. Sivakamasundari V, Lufkin T. Bridging the gap: understanding embryonic intervertebral disc development. Cell Dev Biol. 2012; 1:103. [PubMed: 23106046]
23. Yamanaka Y, Tamplin OJ, Beckers A, Gossler A, Rossant J. Live imaging and genetic analysis of mouse notochord formation reveals regional morphogenetic mechanisms. Dev Cell. 2007; 13:884–896. [PubMed: 18061569]
24. McCann MR, Tamplin OJ, Rossant J, Séguin CA. Tracing notochord-derived cells using a Noto-cre mouse: implications for intervertebral disc development. Dis Model Mech. 2012; 5:73–82. [PubMed: 22028328]
25. Moore ER, Jacobs CR. The primary cilium as a signaling nexus for growth plate function and subsequent skeletal development. J Orthop Res. 2017

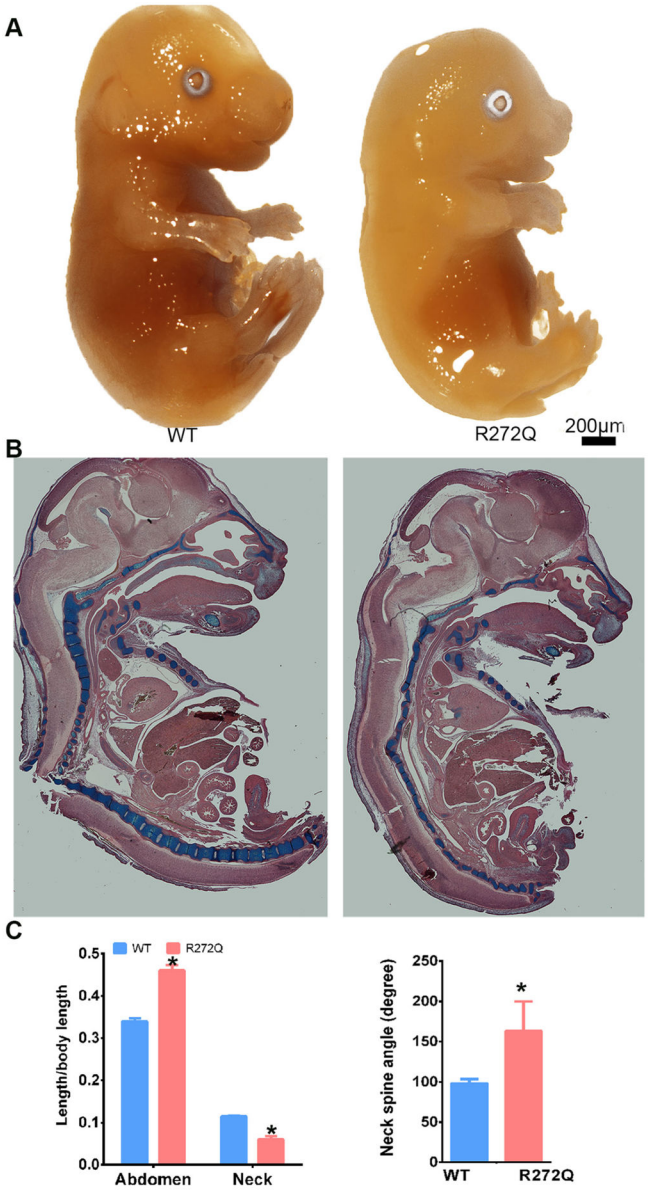

Fig. 1.

Gross morphological abnormalities of *Ick* R272Q homozygous mutant. **a** Sagittal views of wild type (WT) and *Ick* mutant (R272Q) littermate at E15.5. **b** Alcian blue and Picrosirius red staining showing distorted spine in *Ick* mutant at E15.5 as compared with WT littermate. **c** Quantification data indicating significantly increased abdominal length, decreased neck length, and increased neck-spine angle in *Ick* mutant embryos. Data shown as mean ± SEM, $*p < 0.05$ WT vs *Ick* mutant, $n = 3$

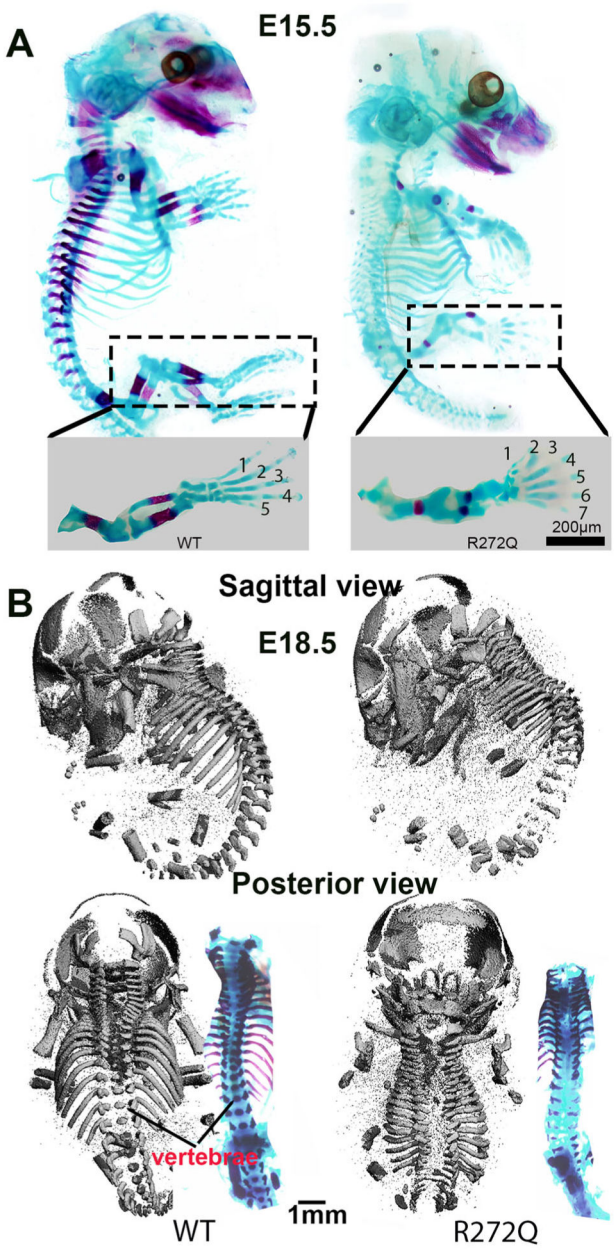

Fig. 2.

Skeletal defects of *Ick* R272Q homozygous mutant. **a** Whole mount skeletal staining of E15.5 embryos of WT and *Ick* mutant using Alizarin red S (calcified tissue in red) and Alcian blue (cartilage tissue in blue). Note, *Ick* R272Q embryos showed polydactyly, reduced mineralization (red), as well as bowed long bones. **b** Representative micro-CT images showing severe defects in vertebrae and spinal processes of E18.5 *Ick* R272Q embryos compared with WT littermates

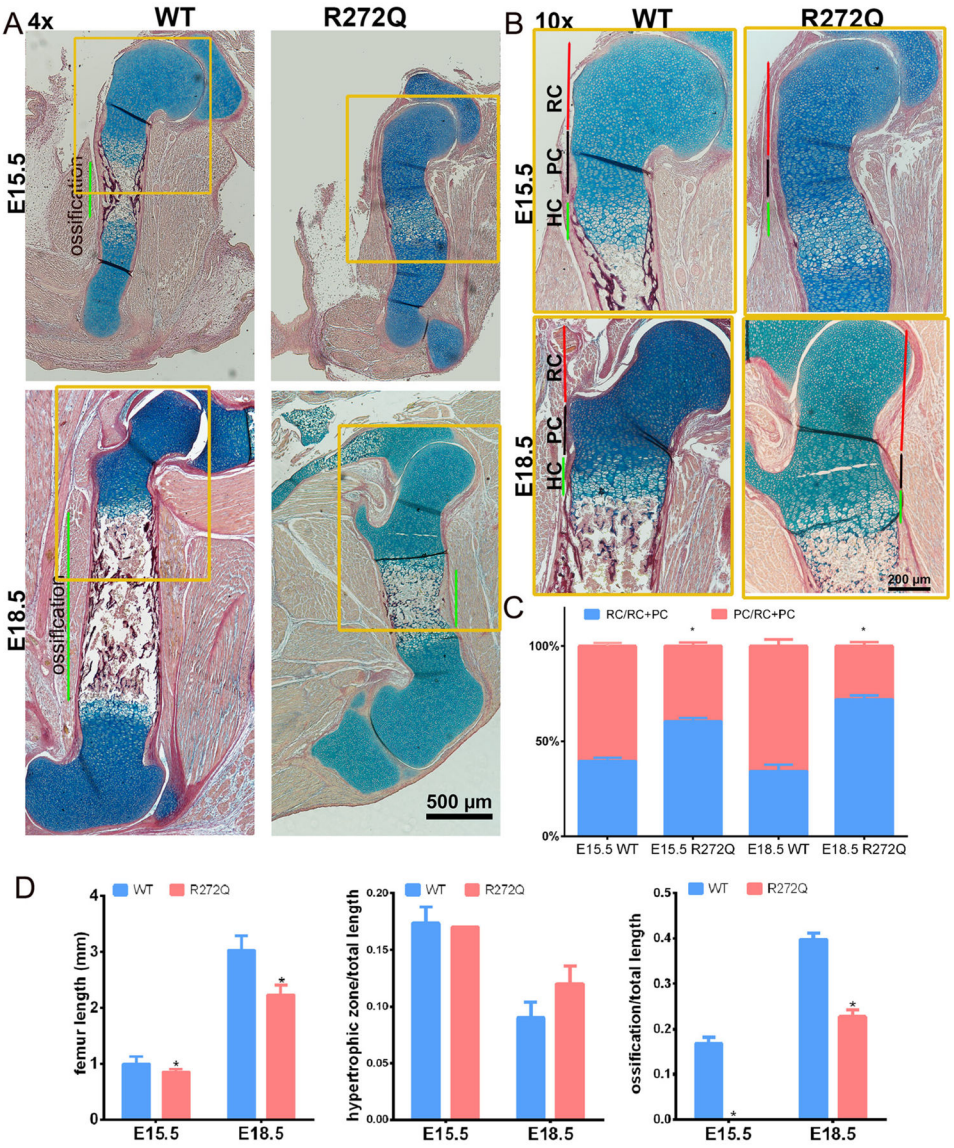

Fig. 3.

Bone ossification is significantly reduced in *Ick* R272Q mutant femurs. Paraffin embedded femoral sections were stained with Alcian blue and Picrosirius red. Shown are representative images of femurs from WT and *Ick* R272Q mutant embryos at E15.5 and E18.5 (**a**, 4 × images; **b** 10× images of boxed areas in **a**). The different chondrocyte zones (marked in **b**) were defined by cell morphology. Quantification data indicating the proportion of resting (RC) and proliferating chondrocyte (PC) zones were shown as mean ± SEM, *$p < 0.05$, WT vs *Ick* mutant, $n = 4$ (**c**). Note that at E15.5, hypertrophic chondrocytes located in the ossification center of *Ick* mutant embryos, whereas mineralized bone formed in the WT control. At E18.5, bone ossification was observed in *Ick* mutant, but the length of the ossification area was much shorter than that in WT littermate. Quantification data of the femur length and the proportion of hypertrophic zone and ossification zone in total bone

length were shown in **d**. Detailed measurement can be found in Online Resource 1. Data shown as mean ± SEM, $*p < 0.05$ WT vs *Ick* mutant, $n = 4$

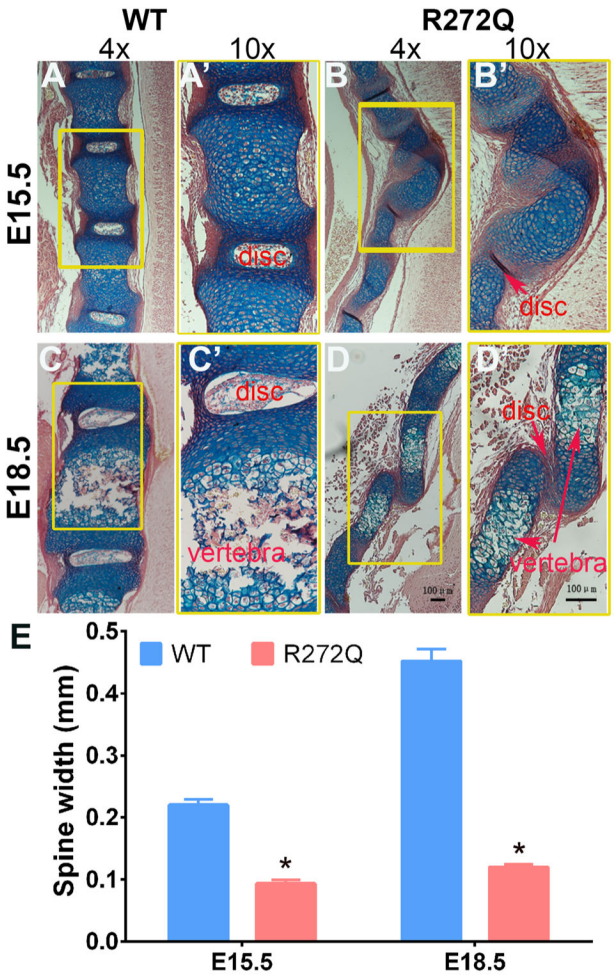

Fig. 4.

Ick mutant spine shows structural defects in the spinal column and intervertebral disks. Shown were representative images of spines (E15.5, **a, b**; E18.5, **c, d**) from WT (**a, a′**; **c, c′**) and R272Q mutant (**b, b′**; **d, d′**) embryos. In *Ick* mutant spine, only premature chondrocytes (E15.5) or hypertrophic chondrocytes (E18.5) located in the spinal ossification center. The width of spinal column was much narrower in *Ick* mutants than in their WT littermates. Shown were quantification data of spine width (**e**), measured as shown in Online Resource 1. Data shown as mean ± SEM, *$p < 0.05$ WT vs *Ick* mutant, $n = 3$

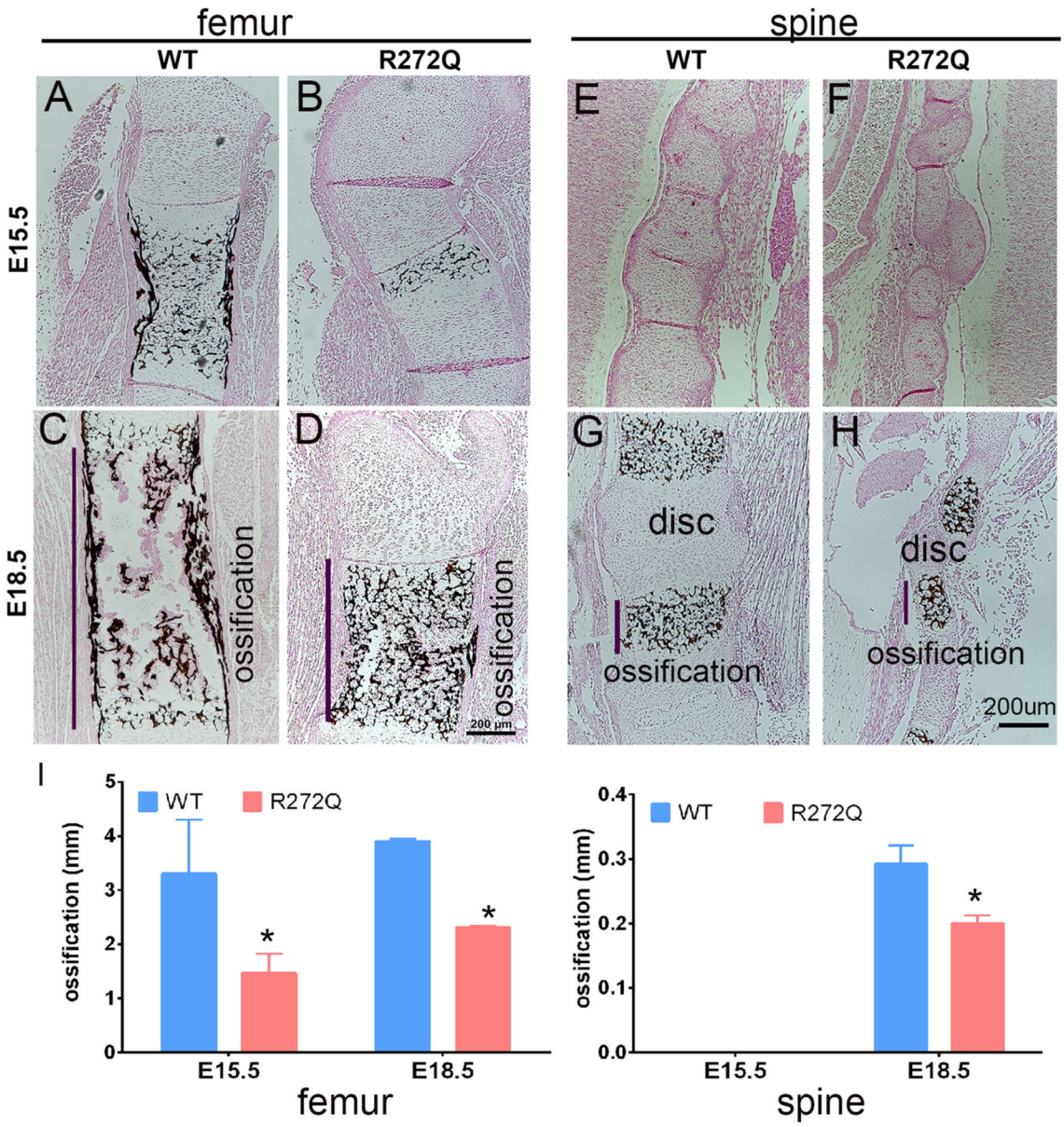

Fig. 5.

Mineralization of spinal column and femur is severely impaired in *Ick* mutant embryos. Paraffin embedded sections of femur (E15.5, **a, b**; E18.5, **c, d**) and spine (E15.5, **e, f**; E18.5, **g, h**) from WT and R272Q mutant embryos were stained by von Kossa showing mineralized bone in black. Note that in E18.5 embryos, significantly less mineralization of femur and spine was observed in *Ick* mutant than in WT control. Shown were quantification data of ossification length (mm) in femur and vertebra (**i**). Detailed measurement can be found in Online Resource 1. Data shown as mean ± SEM, *$p < 0.05$ WT vs *Ick* mutant, $n = 3$

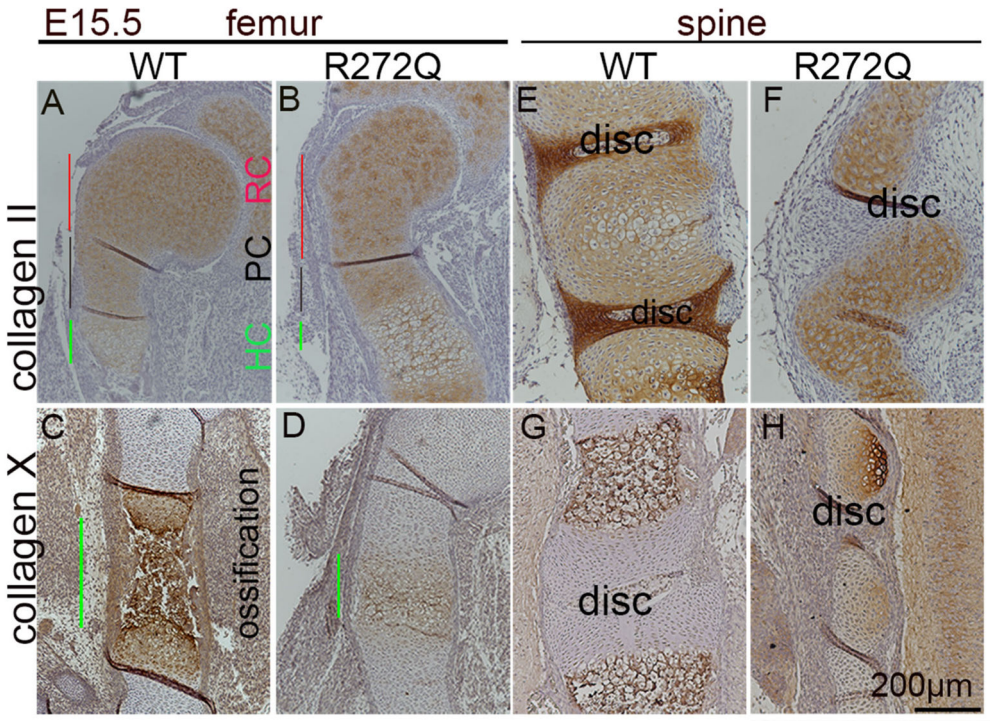

Fig. 6.

Loss of ICK functions significantly alters chondrocyte differentiation and maturation in femur and spinal column. Paraffin embedded sections from spinal columns and femurs of E15.5 WT and R272Q mutants were immunostained for collagen II (a marker for chondrocytes. **a, b, e, f** or collagen X (a marker for hypertrophic chondrocytes, **c, d, g, h**). Note that in the spinal and femur ossification centers of *Ick* mutant embryos, most of the cells were collagen II-positive chondrocytes and collagen X-positive hypertrophic chondrocytes were barely detectable (spine, **h**) or markedly reduced (femur, **d**) compare with WT controls